

Cite this: DOI: 10.1039/xxxxxxxxxxx

SI: Strength of Fluid-filled Soft Composites Across the Elastofracture Length

Christopher W. Barney,^{a,b} Megan T. Valentine,^{b‡} and Matthew E. Helgeson^{a‡}

Received Date
Accepted Date

DOI: 10.1039/xxxxxxxxxxx

www.rsc.org/journalname

1 Mechanical Characterization of Hydrogels

1.1 Pure Shear Notch Tests

Pure shear notch tests were used to characterize $\frac{G_c}{E}$ in hydrogels that did not contain any droplets. Pure shear notch tests were performed in a manner adapted from Rivlin and Thomas.¹ Frames were constructed of 2 glass slides placed 12 mm apart and held in place with tape supports. Films approximately 35 mm in width were then placed into the frame and glued to each slide. The frame was then loaded into tensile fixtures which were clamped onto the glass slides. The tape was then cut with scissors to remove the support and the samples were notched with a razor blade before being stretched to failure at a rate of 0.1 mm/s. This frame, shown in Figure S1, approach was necessary as the samples were found to be extremely brittle and could not be clamped into traditional pure shear fixtures without destroying the films. Due to this brittleness, the samples were not stretched through an initial unnotched cycle to determine a strain energy density function W . Rather it was assumed that the NeoHookean model was appropriate to model for the constitutive response. Due to the low extensibility of these materials ($\sim 5\%$), it could be argued that assuming a Hookean response would be appropriate; however, the NeoHookean model collapses to Hookean behavior at small strains. $\frac{G_c}{E}$ can be calculated from the initial sample height h_o and the critical stretch λ_c .

$$G_c = h_o W(\lambda_c) = \frac{h_o E}{6} (\lambda_c^2 + \lambda_c^{-2} - 2)$$
$$\frac{G_c}{E} = \frac{h_o}{6} (\lambda_c - \lambda_c^{-1})^2 \quad (1)$$

Using this approach, it was found that $\frac{G_c}{E} = 6.5 \pm 3.4 \mu\text{m}$ which indicates that this is an extremely brittle material. The elastofracture length is typically defined as the size scale below which lin-

ear elastic fracture mechanics (LEFM) breaks down and the onset of nonlinear fracture phenomena, such as crack blunting, is observed.² This measurement indicates that this highly crosslinked hydrogel is sensitive to defects on the size scale of a few microns compared to most polymer networks which are typically only sensitive to defects on the order of 100 μm to several millimeters.

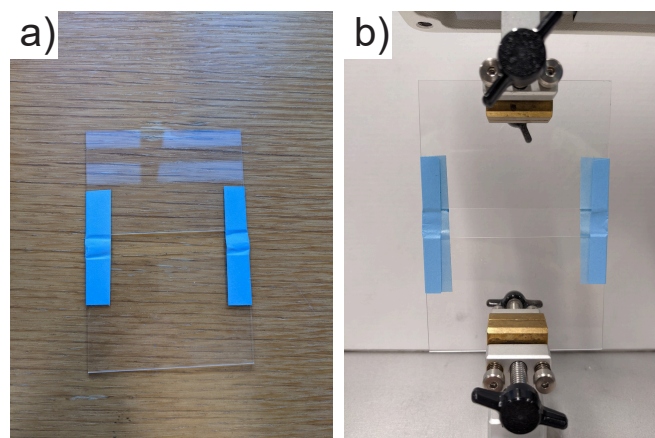


Fig. S1 Images showing an example frame used for pure shear notch tests a) by itself and b) clamped in the fixture.

^aDepartment of Chemical Engineering, University of California Santa Barbara, Santa Barbara CA 93106 USA ^bDepartment of Mechanical Engineering, University of California Santa Barbara, Santa Barbara CA 93106 USA. E-mail: valentine@engineering.ucsb.edu; helgeson@ucsb.edu

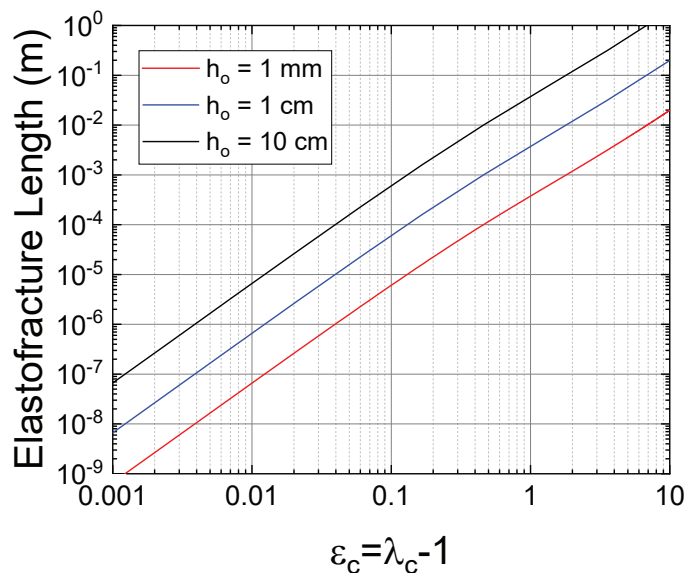


Fig. S2 Plot of $\frac{G_c}{E}$ against failure strain in the presence of a critical defect. Curves are for different initial sample sizes calculated using Equation (1).

1.2 Interpreting $\frac{G_c}{E}$

Another physical interpretation of the elastofracture length, that arises from the form of Equation (1), is that it is a ratio of materials properties that indicate the extensibility of a material in the presence of a critical defect. Here a critical defect is defined as any defect in the material that is equal to or greater in size than $\frac{G_c}{E}$. Since $\frac{G_c}{E}$ is measured from materials properties, in some cases, it may be a more reliable indicator of brittleness than the failure strain of unnotched samples. A plot of the elastofracture length, assuming a NeoHookean constitutive response, against the failure strain in the presence of a critical defect for different sample sizes is contained in Figure S2. This graph allows one to compare the brittleness of different materials with a parameter that is easily understood, i.e. how much the material can be stretched in the presence of a critical defect. For example, when $h_o = 1$ cm materials with $\frac{G_c}{E} = \{1, 10, 100, 1000\}$ μm could be stretched to $\varepsilon_c = \{1, 4, 10, 50\}$ % before failing in the presence of a critical defect.

Notably, the $\frac{G_c}{E}$ value of a few microns measured for the hydrogels, without added droplets, used in this study indicates that these samples can only be strained a few percent before failure occurs. In the composite hydrogels, 1/3 of the volume of these hydrogels are replaced with a low viscosity silicone oil that lacks the network structure needed to bear stress. As a result, $\frac{G_c}{E}$ of the composite hydrogels should decrease and these materials should be more brittle relative to the hydrogels without droplets. This is consistent with the experimental observations that composite hydrogel samples were too brittle to transfer onto the glass slide frame used to quantify fracture in the hydrogels without droplets. Due to this increase in brittleness, puncture was used to evaluate the failure of composite hydrogels, as described in the main text. An image and schematic of these samples is contained in Figure S3.

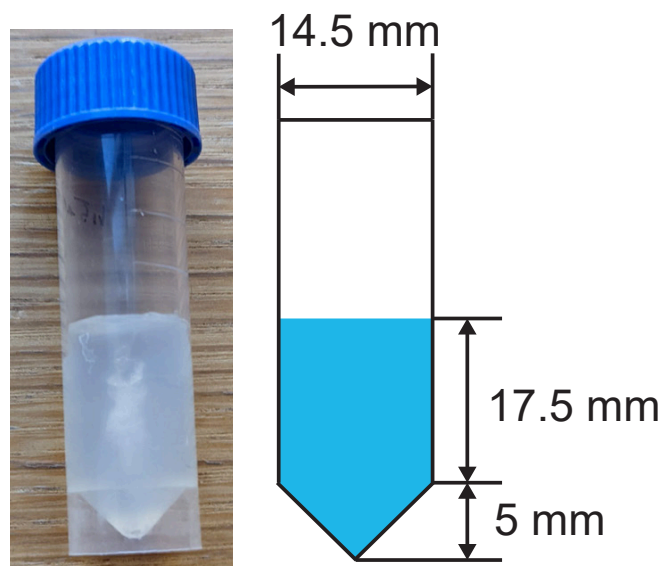


Fig. S3 Image and schematic of the samples used to perform puncture measurements on the composite hydrogels. For each measurement, 3 mL of material was tested in a 5 mL vial with a conical base and an internal diameter of ~ 14.5 mm. The height of the sample filled above the bottom cone was ~ 17.5 mm while the height of the cone was ~ 5 mm, as shown. In all cases, samples were punctured with a 2 mm diameter flat steel cylinder at a rate of 0.1 mm/s.

1.3 Rheological Characterization

Rheological characterization of a subset of the gels used in this study was performed on a TA Instruments AR-G2 stress-controlled rheometer with a UV LED array and transparent 20 mm diameter parallel plate fixtures with a gap size of 500 μm to allow for simultaneous UV exposure and rheological measurement. These experiments were performed to establish a baseline value for the modulus of the hydrogel phase in the absence of nanoemulsion droplets, and check whether the E values measured via indentation were reasonable. Experiments were performed on the hydrogel both with and without any added silicone oil droplets. In the former case, measurements were performed at room temperature resulting in dispersed droplets corresponding to $L_c = 25.2$ nm. The curing profile was monitored by exposing the sample to 300s of UV irradiation (1 mW/cm²) while simultaneously monitoring the mechanical response using small amplitude oscillatory shear measurements with an amplitude strain of 0.1% and a frequency of 10 rad/s. Properties of the hydrogel were monitored for an additional 300 s after UV exposure to ensure that stable properties developed and any residual curing was finished. Then the time-dependent responses of the materials were probed with frequency sweeps. A strain amplitude of 0.1% and frequencies ranging from 0.1 rad/s to 628.3 rad/s were used. All measurements were performed at room temperature (23.9°C). Adjustments to the gap size were enabled based on maintaining a nominal normal force (which was zeroed immediately before measurements were initiated) of 0 N, tracking this value with a sensitivity to values exceeding 0.1 N.

Plots showing the curing profile and frequency sweep data for the hydrogel without any added silicone oil droplets is shown in

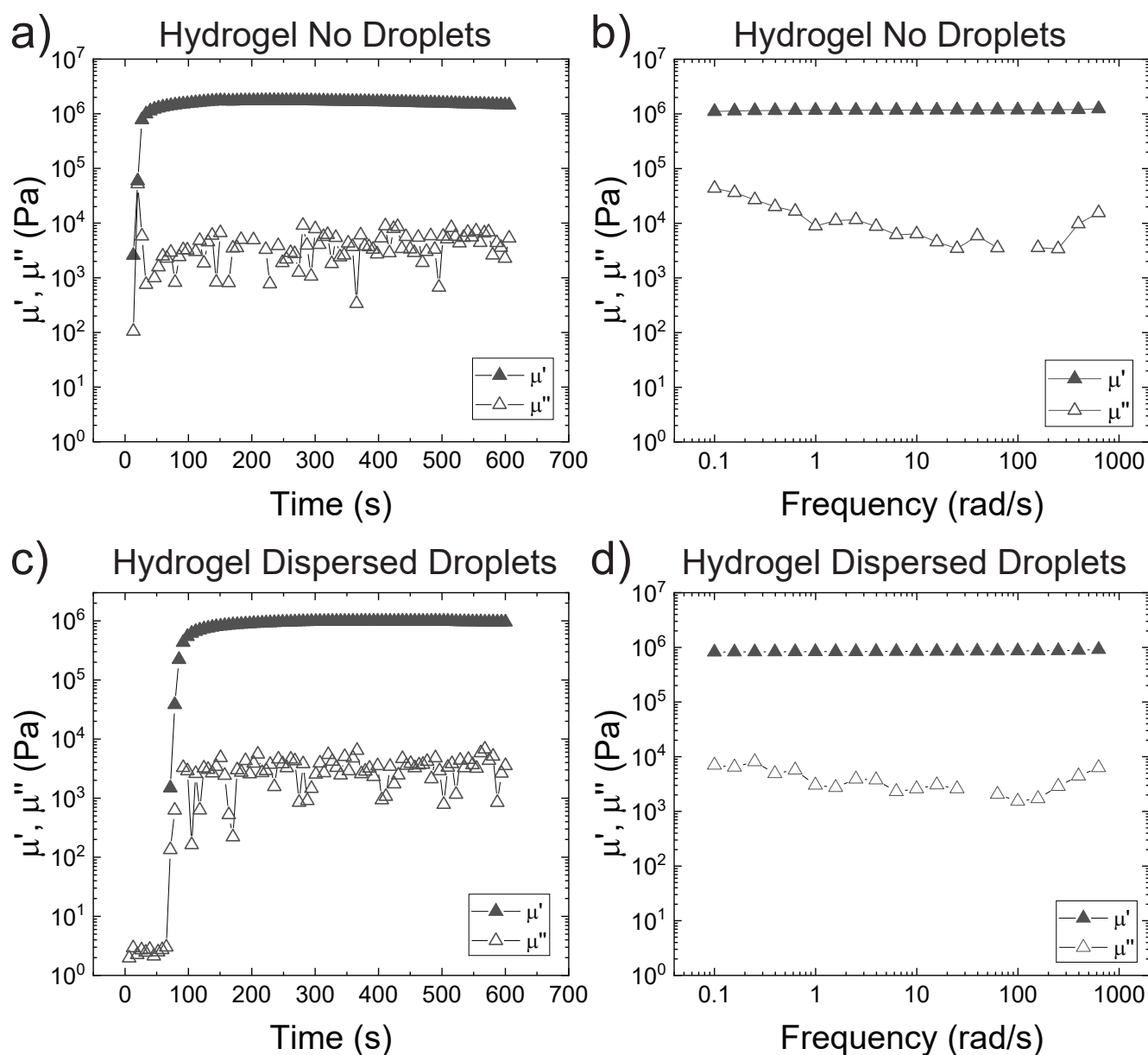


Fig. S4 Plots showing the curing profile and storage μ' and loss μ'' shear moduli obtained using frequency sweep measurements in the small strain regime (0.1% strain) performed on a-b) hydrogels that contain no droplets and c-d) hydrogels containing dispersed droplets with an $L_c = 0.0252 \mu\text{m}$.

Figure S4(a-b). The precursor solution for this hydrogel is composed of 33 vol.% of a 700 g/mol PEGDA. The remainder of the solution is composed of water and surfactant (SDS is incorporated at a concentration of 200 mM in reference to the total solution volume, which is the same as is contained in the nanoemulsion samples). The curing profile for this hydrogel shows that the solution rapidly gels upon UV exposure as evidenced by the fact that the shear storage modulus μ' exceeds the shear loss modulus μ'' at the first data point gathered at 13 s. μ' then increases and eventually plateaus in the MPa range. The frequency sweeps indicate that this hydrogel is highly elastic with μ' exceeding μ'' by 1-2 orders of magnitude across the entire range of frequencies measured. These sweeps also show that μ' is largely insensitive to frequency in these gels, with a range of values from 1.10 MPa

at 0.1 rad/s to 1.24 MPa at 628.3 rad/s with an average value of 1.2 MPa. Conversion between shear and Young's moduli can be performed through

$$E = 2(1 + \nu)\mu \quad (2)$$

where ν is Poisson's ratio. Assuming that this hydrogel is incompressible sets $\nu = 0.5$, giving a predicted value of $E = 3.6 \text{ MPa}$ for the hydrogel phase.

Plots showing the curing profile and frequency sweep data for the hydrogel with added silicone oil droplets is shown in Figure S4(c-d). These gels have an L_c value of 25.2 nm based on the radius of the droplets which were incorporated at 33 vol.%. The curing profile for this hydrogel shows that the solution gels after approximately 70 s of UV exposure. This delay in gelation

time relative to the pure hydrogel is likely attributable to the additional scattering of UV rays at the droplet interfaces. μ' then increases and eventually plateaus slightly below the MPa range. The frequency sweeps indicate that this hydrogel is highly elastic with μ' exceeding μ'' by 2 orders of magnitude across the entire range of frequencies measured. These sweeps also show that μ' is largely insensitive to frequency in these gels, with a range of values from 0.82 MPa at 0.1 rad/s to 0.92 MPa at 628.3 rad/s with an average value of 0.85 MPa. This gives a value of $E = 2.55$ MPa which falls well within the $E = 2.5 \pm 0.3$ MPa range measured via indentation, as described in the main text.

2 Estimating Surface Strains At Puncture

One simple, but insufficient, method of estimating the failure strain at puncture is to normalize the contact force during indentation with a flat cylindrical indenter to get a nominal stress.

$$F = \frac{8}{3}ERd$$

$$\sigma = \frac{8}{3\pi}E\frac{d}{R} \quad (3)$$

This takes the familiar form of a stress-strain relationship where the stress is related to a geometry-specific constant coefficient, the elastic modulus, and a ratio of size scales in the system that represent strain. Noting that the observed puncture displacements are on the same order of magnitude as the indenter radius suggests that $\frac{d_c}{R} \approx 100\%$. However, this cannot be an accurate reflection of the failure strain, as the gels studied here were extremely brittle, which did not allow for conventional clamping and notching and required puncture tests in the first place. This apparent discrepancy arises from the fact that, while the stress-strain relationship takes a familiar form, indentation involves a complex, non-uniform deformation field where the local strains are not well approximated by $\frac{d_c}{R}$. Instead it is more appropriate to estimate the failure strains by calculating the local surface strains observed in the system.

The tangential surface displacements experienced in a material subjected to a uniform displacement over a circular area is given by,³

$$u_r = -\frac{(1-2\nu)}{(1-\nu)}\frac{d}{\pi}\left[\frac{a}{r} - \left(\frac{a^2}{r^2} - 1\right)^{1/2}\right], \quad r \leq a,$$

$$u_r = -\frac{(1-2\nu)}{(1-\nu)}\frac{d}{\pi}\frac{a}{r}, \quad r > a, \quad (4)$$

where u_r represents displacement in the radial direction within the surface, a represents the contact radius, and r represents the distance from the center of the contact area. From this the surface strains can be calculated.

$$\epsilon_\theta = \frac{u_r}{r} = -\frac{(1-2\nu)}{(1-\nu)}\frac{d}{\pi r}\left[\frac{a}{r} - \left(\frac{a^2}{r^2} - 1\right)^{1/2}\right], \quad r \leq a$$

$$\epsilon_\theta = \frac{u_r}{r} = \frac{(1-2\nu)}{(1-\nu)}\frac{d}{\pi}\frac{a}{r^2}, \quad r > a \quad (5)$$

$$\epsilon_r = \frac{\partial u_r}{\partial r} = \frac{(1-2\nu)}{(1-\nu)}\frac{d}{\pi}\left[\frac{a}{r^2} - \frac{a^2}{r^3}\left(\frac{a^2}{r^2} - 1\right)^{-1/2}\right], \quad r \leq a$$

$$\epsilon_r = \frac{\partial u_r}{\partial r} = \frac{(1-2\nu)}{(1-\nu)}\frac{d}{\pi}\frac{a}{r^2}, \quad r > a \quad (6)$$

Since plane strain conditions occur at the corner of the punch and ϵ_z is obviously compressive, one of the surface strains will be compressive and the other tensile. As $u_z = d$ inside of the contact area, there are no shear strains meaning that the two surface strains are principal strains. Plugging $r = a$ into ϵ_θ shows that it is unambiguously negative. Doing the same for ϵ_r shows that it is composed of two terms. The first term represents the extensional component of the strain, and is equivalent to the ϵ_r outside of the contact area. The second term diverges to $-\infty$ as $r \rightarrow a$, and is associated with hydrostatic compression below the probe and would not drive failure. Calculating the extensional strain when $r = a$ gives

$$\epsilon_r = \frac{(1-2\nu)}{(1-\nu)}\frac{d}{\pi a}. \quad (7)$$

Note that since $a = R$ the tensile strain at the edge of contact is partly determined by $\frac{d}{R}$. Setting $\frac{d}{R} = 1$ and estimating $\nu = 0.49$ gives a value of $\epsilon_r = 0.0125$, indicating a strain of approximately 1.25% at the corner of the probe when puncture occurs. This is well below the value of 100% that is suggested when estimating the strain by just taking $\frac{d_c}{R}$. Taking the maximum observed puncture displacement (2.301 mm) gives a strain of 2.87%, indicating that failure is observed at strains around 1-3% in this study, which is physically consistent with their extremely brittle nature..

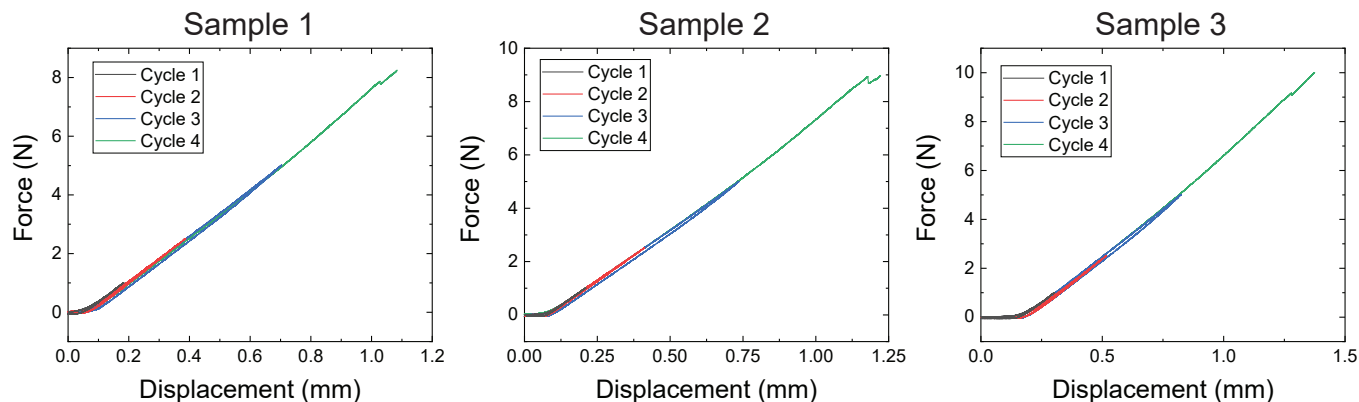


Fig. S5 Plots showing the force displacement relationship of three different dispersed droplet samples with $L_c = 0.0252$ nm. The low hysteresis values indicate that this is a highly elastic deformation process.

3 Puncture Measurement Controls

3.1 Cyclic Loading

Cyclic loading was used to quantify the reversibility of the deep indentation measurement. Measurements were made on three dispersed droplet samples with $L_c = 0.0252$ nm. Cycles 1-3 were run at a displacement rate of $10 \mu\text{m/s}$ to a turnaround force of 1, 2.5, and 5 N respectively. The fourth "cycle" was run to puncture of the material. Plots of the observed force-displacement relationships during cyclic loading are shown in Figure S5. These curves indicate that the deep indentation process displays little hysteresis and is highly elastic. On the third cycle, $93.9 \pm 0.7\%$ of the energy input into the system during deformation is recovered upon unloading. The small amount of energy dissipated during deformation is likely caused by a Mullins softening effect of breaking chains in the network.

3.2 Puncture Speed

The influence of the displacement speed on the puncture was quantified and is shown in Figure S6. The data at 0.01 and 1 mm/s were taken on dispersed droplet gels with $L_c = 25.2$ nm and the data at 0.1 mm/s were taken on dispersed droplet gels with $L_c = 24.1$ nm. This plot shows a slight dependence between the two properties with the puncture force scaling with displacement rate to the 0.11 power. This is reasonably consistent with past measurements in soft gels that found a 0.20 scaling between these two properties.⁴

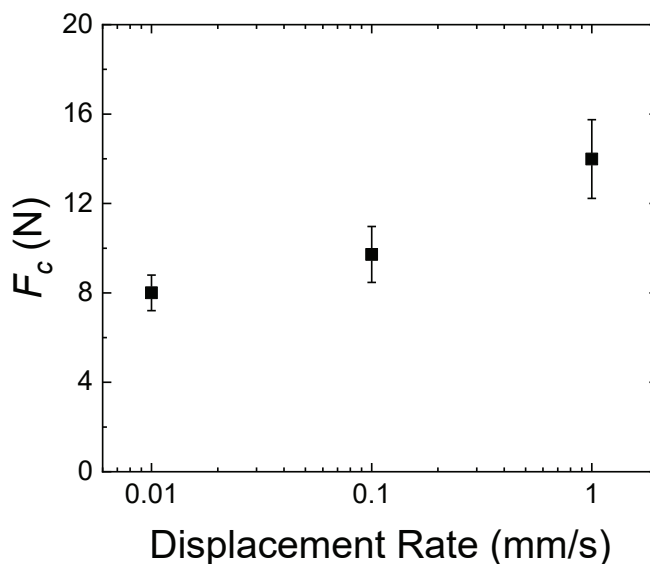


Fig. S6 Plot showing the puncture force against displacement rate for dispersed droplet samples with $L_c = 25.2$ nm at displacement rates of 0.01 and 1 mm/s and $L_c = 24.1$ nm. The data shows a slight dependence with puncture force scaling with displacement rate to the 0.11 power.

Table 1 Summary of the data gathered on the composite hydrogel systems in this work.

Sample	L_c (μm)	R (mm)	d_c (mm)	F_c (N)	E (MPa)	$\frac{\sigma_c}{E}$
24_1drop-1	0.0241	1	1.382	8.514	2.14	1.2687
24_1drop-2	0.0241	1	1.538	9.193	2.13	1.3718
24_1drop-3	0.0241	1	1.679	11.442	2.33	1.5629
33_2drop-1	0.0332	1	1.821	13.565	2.80	1.5417
33_2drop-2	0.0332	1	2.301	16.950	2.88	1.8751
33_2drop-3	0.0332	1	1.226	7.488	2.68	0.8905
50_8drop-1	0.0508	1	1.078	7.718	2.64	0.9335
50_8drop-2	0.0508	1	1.468	12.306	2.88	1.3648
50_8drop-3	0.0508	1	1.045	7.663	2.71	0.9043
73_6drop-1	0.0736	1	1.069	7.145	2.30	0.9906
73_6drop-2	0.0736	1	0.6599	3.929	2.16	0.5788
73_6drop-3	0.0736	1	0.747	4.939	2.44	0.6452
0_90gel-1	0.90	1	1.043	4.897	1.59	0.9789
0_90gel-2	0.90	1	0.770	3.977	1.94	0.6524
0_90gel-3	0.90	1	1.455	7.994	1.87	1.3629
1_47gel-1	1.47	1	0.662	3.238	1.86	0.5538
1_47gel-2	1.47	1	0.870	3.898	1.83	0.6795
1_47gel-3	1.47	1	0.625	3.122	1.93	0.5150
4_65gel-1	4.65	1	0.903	3.031	1.26	0.7653
4_65gel-2	4.65	1	0.947	3.343	1.28	0.8283
4_65gel-3	4.65	1	0.987	3.204	1.15	0.8860
5_80gel-1	5.80	1	0.628	2.756	1.92	0.4573
5_80gel-2	5.80	1	0.835	3.866	1.81	0.6790
5_80gel-3	5.80	1	0.854	3.887	2.03	0.6092
6_03gel-1	6.03	1	1.166	4.044	1.26	1.0199
6_03gel-2	6.03	1	0.770	2.693	1.41	0.6098
6_03gel-3	6.03	1	0.968	3.451	1.37	0.8022
6_20gel-1	6.20	1	0.723	2.9423	1.50	0.6225
6_20gel-2	6.20	1	0.806	2.5895	1.31	0.6313
7_20gel-1	7.20	1	0.872	3.914	1.77	0.7050
7_20gel-2	7.20	1	0.836	3.760	1.71	0.6991
7_20gel-3	7.20	1	0.771	3.602	1.89	0.6081
25_1gel-1	25.1	1	0.786	3.254	1.84	0.5621
25_1gel-2	25.1	1	0.756	3.566	1.95	0.5824
25_1gel-3	25.1	1	0.818	3.486	1.73	0.6430
34_6gel-1	34.6	1	0.733	2.810	1.87	0.4770
34_6gel-2	34.6	1	0.768	3.054	1.72	0.5647
34_6gel-3	34.6	1	0.780	3.232	1.96	0.5248

References

- 1 R. S. Rivlin and a. G. Thomas, *Journal of Polymer Science*, 1953, **10**, 291–318.
- 2 C. Creton and M. Ciccotti, *Reports on Progress in Physics*, 2016, **79**, 046601.
- 3 J. W. Harding and I. N. Sneddon, *Mathematical Proceedings of the Cambridge Philosophical Society*, 1945, **41**, 16–26.
- 4 S. Rattan and A. J. Crosby, *Extreme Mechanics Letters*, 2018, **24**, 14–20.